Kinetic Modeling of Counterflow Diffusion Flames of Butadiene

SILVIA GRANATA, TIZIANO FARAVELLI, and ELISEO RANZI*

CMIC Dipartimento di Chimica, Materiali e Ingegneria Chimica, Politecnico di Milano, Milano, Italy

and

NESRIN OLTEN and SELIM SENKAN

Department of Chemical Engineering, University of California, Los Angeles, CA, USA

A comprehensive, semi-detailed kinetic scheme was used to simulate the chemical structures of counterflow diffusion and fuel-rich premixed 1,3-butadiene flames, to better understand the formation of polycyclic aromatic hydrocarbons (PAH). The results showed that model predictions were in good agreement with the experiments for most of the species in both the flames. In the counterflow flames higher-molecular weight products are slightly over predicted. The pathways characterizing the pollutant formation are very different in the premixed and in the counterflow flames confirming or suggesting the need to verify and refine the detailed mechanisms tuned for premixed conditions when they are extrapolated and used in diffusion flames. Reaction paths analysis for PAH formation in the counterflow flame shows that both the HACA mechanism and the resonantly stabilized radicals are important for the growth of PAH. The kinetic model was unsuccessful in predicting the increased reactivity in O_2-doped diffusion flames, indicating the need for improved models and also the opportunity of new experiments of butadiene oxidation in the intermediate temperature region. © 2002 by The Combustion Institute

INTRODUCTION

1,3-butadiene is an important intermediate produced in large quantities in hydrocarbon flames. Also, butadiene flames soot more readily than flames of some aromatic hydrocarbons [1]. In addition, it also polymerizes in the gas-phase even at moderate temperatures [2–4]. This lead some researchers [5–7] to propose the Diels-Alder additions to 1,3-butadiene, acetylene and other olefins as primary routes to six-carbon ring compounds, aromatic hydrocarbons and polycyclic aromatic hydrocarbons (PAH). These reactions were also advocated to play an important role in the undesired successive polymerizations of ethylene in steam cracking process which ultimately lead to coke formation [8]. However, Diels-Alder reactions subsequently were determined to be too slow to account for the formation of aromatics in the flames [9]. Regardless of all these arguments, the fact that 1,3-butadiene and other four carbon intermediates (e.g., vinylacetylene, biacetylene) form in all the flames and are nearly identical in shape and position to PAH motivates this study.

Recently the detailed structure of the counterflow diffusion flame of 1,3-butadiene was experimentally investigated with and without partial oxygen addition to the fuel side by Olten and Senkan [10]. Major, minor and trace species mole fraction profiles were measured up to pyrene (202 Daltons) in the case of pure 1,3-butadiene flame and cyclopenta(cd)pyrene and its isomer benzo(ghi)fluorantene (226 Daltons) in oxygen doped counterflow diffusion flame. In an earlier study, the near sooting premixed flat flame of 1,3-butadiene was also investigated [9].

In this study, we compare the predicted and the experimental profiles for these counterflow flames and the premixed flame with the aim of elucidating the competitive reaction paths in different operating conditions.

Model predictions were determined by using the semi-detailed reaction mechanism already presented elsewhere [11]. Another objective of this study was to better understand the role that resonantly stabilized radicals such as C_3H_3 and C_5H_5 play in the formation

of aromatics and soot in 1,3-butadiene combustion [12, 13].

EXPERIMENTAL APPARATUS AND MEASUREMENTS

Counterflow Diffusion Flame

The details of experimental set-up can be found elsewhere [10, 14, 15], thus only a brief description will be provided. The 1,3-butadiene diffusion flame was stabilized between two opposed jet (2.54 cm ID) burners. Screens (100 mesh) were used at the exit of each burner to generate uniform flows for stable, flat flame formation. Argon shield gas was used to protect the flame from surrounding air. The oxidizer stream was 22% O_2 and 78% Ar which was introduced from the upper burner. The fuel stream containing 50% 1,3-C_4H_6 and 50% Ar was introduced from the bottom burner. All gases used were of high purity (99.99%+). Shield gas and combustion products were gently vented from the bottom burner by means of a vacuum pump. Flame sampling was accomplished with a heated quartz micro-probe, followed by online gas analysis using gas chromatography and mass spectrometry [10, 14, 15]. The accuracy of the concentration profiles was estimated to be 15% for species for which calibration standards were available [10]. Otherwise, the accuracy of the measurements should be within a factor of 2 based on the ionization cross section method used [10]. Gas temperature measurements were accomplished by using coated thermocouples and the rapid insertion method [10]. The accuracy of the temperature measurements with this technique are expected to be within 50 to 75 K depending on the temperature, as measurements are taken before significant soot deposits accumulate on the thermocouple surfaces. Clearly radiative heat losses from the thermocouple bead would lower the thermocouple readings in the fuel side of the flame. However, in the air side radiative heat losses should be less. Sampling position within the flame was changed by moving the entire burner assembly vertically up or down with respect to the fixed sampling and thermocouple probes to determine the species and temperature profiles, re-
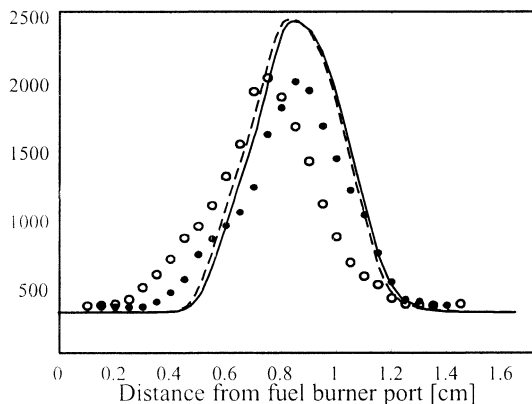

Fig. 1. Experimental (points) and predicted temperature profiles [K] of the counter flow diffusion flames. Solid line and filled symbols refer to the pure diffusion flame, dashed line and empty symbols refer to the partially premixed flame.

spectively. This was accomplished by using vertical and horizontal unislide assemblies having a movement precision of 0.01 mm. Positional accuracy of the concentration and temperature profiles with respect to the burner was estimated to be ±0.25 mm.

Figure 1 shows the temperature profiles along the burner axis and also compares experimental data with model predictions. The latter was determined by solving the energy balance equation under adiabatic conditions. Solid line and filled symbols refer to the pure diffusion flame, while the dashed line and empty symbols refer to the oxygen-doped flame. As can be seen from this figure, although the peak temperatures were overestimated, their peak positions and shapes match well with the experimental data. The over-estimation of the temperature maxima can be partially attributed to the adiabatic nature of the calculations, that is, the absence of heat losses, for example, radiation, in the model.

Laminar Premixed Flame

Experimental data of a nearly sooting laminar premixed flat flame [9] were already analyzed in a recent paper [11]. This flat butadiene flame was produced at the burner chamber pressure of 2.67 kPa (20 torr.) with 52.1 Ncm_s^{3-1} of feed gas, consisting in 29.5 mol% 1,3-butadiene, 67.5 mol% oxygen, 3.0 mol%

argon, corresponding to a fuel equivalence ratio Φ of 2.4 and a cold gas velocity of 0.5 ms^{-1} at 298 K.

MATHEMATICAL MODELING AND COMPARISONS WITH EXPERIMENTAL DATA

Numerical Model

The computational model used in this work is a modified version of the opposed-flow diffusion flame code (OPPDIF) [16] and the premixed flame code (PREMIX) [17]. These modifications allow the use of H abstraction reactions described in a simplified form (which assumes analogy and similarity rules for the estimation of the kinetic parameters) and they also allow flexibility with respect to equivalent or lumped reactions with several products [18].

The base formulation of the one-dimensional opposed-flow diffusion flame assumes two concentric circular nozzles, which produce an axisymmetric flow field. A stagnation plane lies somewhere in between the nozzles and its position depends on the relative mass flow rates of the two streams. The problem is readily reduced to a quasi-one dimensional form, which makes the solution easier, even in the presence of numerous species involved in a detailed kinetics problem. For instance, the radial velocity is assumed to vary linearly in the radial direction, and the temperature and axial velocity are assumed to be constant along the radial coordinates, allowing the fluid properties to be a function of the axial distance only. These simplifications are usually accepted even if they can influence the predictions, particularly in the case of asymmetric flow-fields. Nevertheless, comparisons between the experiments and the model predictions have been usually found to be in good agreement, which suggests that the code can be employed with reasonable confidence [19, 20].

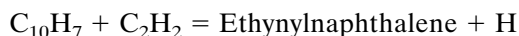### Chemical Kinetic Mechanism and Comparisons with Experimental Data

The kinetic mechanism (SOX 0102) is based on a general approach for the development,

validation and the extension of a single, detailed oxidation scheme for several fuels [18]. Because of the hierarchical modularity of the mechanistic scheme, this model is based on a detailed sub-mechanism of C_1-C_4 species. Assuming analogy rules for similar reactions, only a few fundamental kinetic parameters are required for the progressive extension of the scheme toward heavier species [21]. The resulting kinetic model of hydrocarbon oxidation from methane up to n-tetradecane, jet fuels and diesel oils consists of about 200 species and 3,000 reactions. Almost all the reactions considered in this work were already published in the previous references, the complete scheme is available upon request and it will also be available on the web in the next future. Selected reactions are reported in Table 1. They refer to addition reactions of C_4H_5 on unsaturated species, addition reactions of aromatic radicals on acetylene and also some radical reactions of particular interest and sensitivity in benzene and PAH formation in the analyzed conditions.

Kinetic parameters of C_4H_5 addition reactions on unsaturated species were well tested in pyrolisis conditions [22] and were already discussed by Goldaniga et al. [11]. The proposed kinetic parameters for the addition reactions of aromatic radicals on C_2H_2 are $10^9 \exp(-5000/RT)$ [m^{3}kmol^{-1} s^{-1}]. These values are nearly double of those used for C_4H_5 additions. These reactions are relevant steps in the HACA mechanism and the proposed kinetic values are very close, in the temperature range of interest, to those suggested by Frenklach and adopted in the ABF kinetic model [23]:

$C_6H_5 + C_2H_2 = $ Ethynylbenzene $+ $ H

$\quad$ k $= 3.3 \times 10^{30} T^{-5.7} \exp(-25500/RT)$

$\quad$ [m^{3}kmol^{-1}s^{-1}]

$C_{10}H_7 + C_2H_2 = $ Ethynylnaphthalene $+ $ H

$\quad$ k $= 1.3 \times 10^{21} T^{-3.06} \exp(-22600/RT)$

$\quad$ [m^{3}kmol^{-1}s^{-1}]

Resonant radicals add on double bonds with higher activation energy because of their stability. Recombination reactions of resonantly sta-

TABLE 1

Kinetic Parameters of Relevant Reactions (units are m³, kmol, kcal, s)

Addition Reactions of C_4H_5 on Unsaturated Species

	A	E
$C_4H_5 + C_2H_2$ = Benzene + H	.50E + 09	5000.
$C_4H_5 + C_2H_4$ = Benzene + H + H_2	.25E + 09	7000.
$C_4H_5 + aC_3H_4$ = Benzene + CH_3	.25E + 09	5000.
$C_4H_5 + pC_3H_4$ = Benzene + CH_3	.25E + 09	5000.
$C_4H_5 + C_4H_2$ = Ethynylbenzene + H	.50E + 09	3000.
$C_4H_5 + C_4H_2$ = Benzene + C_2H	.50E + 09	5000.
$C_4H_5 + C_4H_4$ = Benzene + C_2H_3	.50E + 09	5000.
$C_4H_5 + C_4H_4$ = Styrene + H	.25E + 09	5000.
$C_4H_5 + C_4H_6$ = Benzene + H_2 + C_2H_3	.50E + 09	7000.
$C_4H_5 + C_4H_6$ = Toluene + CH_3	.10E + 09	7000.
$C_4H_5 + C_4H_6$ = Styrene + H_2 + H	.10E + 08	7000.
$C_4H_5 + Benzene$ = Naphthalene + H_2 + H	.50E + 09	3000.
Addition Reactions of Aromatic Radicals on Acetylene		
$C_2H_2 + C_6H_4CH_3$ = Indene + H	.10E + 10	5000.
$C_2H_2 + C_8H_5 = C_{10}H_7$	.10E + 10	5000.
$C_2H_2 + C_8H_7$ = Naphthalene + H	.10E + 10	5000.
$C_2H_2 + C_{10}H_7$ = Acenaphthylene + H	.05E + 10	5000.
$C_2H_2 + C_{12}H_9$ = Phenanthrene + H	.10E + 10	5000.
$C_2H_2 + C_{14}H_9$ = Pyrene + H	.10E + 10	5000.
$C_2H_2 + C_{16}H_9 = C_{18}H_{10}^{*}$ + H	.10E + 10	5000.
(Resonantly stabilized radicals)		
$C_2H_2 + C_7H_7$ = Indene + H	.20E + 10	24000.
$C_2H_2 + C_9H_7 = C_{11}H_9$	.20E + 10	24000.
$C_2H_2 + C_{11}H_9$ = Acenaphthylene + CH_3	.20E + 10	24000.
Radical-Radical Reactions		
$C_3H_3 + C_3H_3$ > Benzene	.30E + 10	0.
$C_3H_3 + C_3H_3 > C_6H_5$ + H	.30E + 10	0.
$C_3H_3 + C_7H_7$ > Naphthalene + H + H	.50E + 09	0.
$C_3H_3 + C_{11}H_9$ > Phenanthrene + H + H	.50E + 09	0.
$C_3H_3 + C_{14}H_9 > C_{17}H_{12}^{*}$	.50E + 09	0.
$C_3H_3 + C_{16}H_9 > C_{19}H_{12}^{*}$	.50E + 09	0.
$C_5H_5 + C_5H_5$ > Naphthalene + H + H	.50E + 09	0.
$C_5H_5 + C_7H_7$ > Biphenyl + H + H	.20E + 09	0.
$C_5H_5 + C_{16}H_7 > C_{15}H_{12}^{*}$	.20E + 09	0.
$C_5H_5 + C_{14}H_9 > C_{19}H_{14}^{*}$	.20E + 09	0.
$C_5H_5 + C_{10}H_9 > C_{21}H_{14}^{*}$	.20E + 09	0.

Species marked with the * are equivalent components delumped into reference species

bilized radicals play an important role in the aromatic ring formation and growth. The proposed rate constants are derived from the values of the model propargyl recombination reaction [12]

$C_3H_3 + C_3H_3$ = Benzene
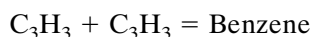
$k = 3 \times 10^9 [m^3 kmol^{-1} s^{-1}]$.

The thermochemical information were primarily obtained from the CHEMKIN thermodynamic database [24, 25]. Unavailable thermodynamic data were estimated by group additivity methods [26]. Transport properties were taken from the CHEMKIN transport database [27] or estimated following the procedure proposed by Wang and Frenklach [28].

Figure 2 shows a detailed comparison of experimental data and model predictions for counterflow diffusion flame of pure 1,3-butadiene. Model predictions are carried out assuming adiabatic temperature profiles. It should be noted that similar results were also obtained when 3% of oxygen was added to the fuel stream. As previ-
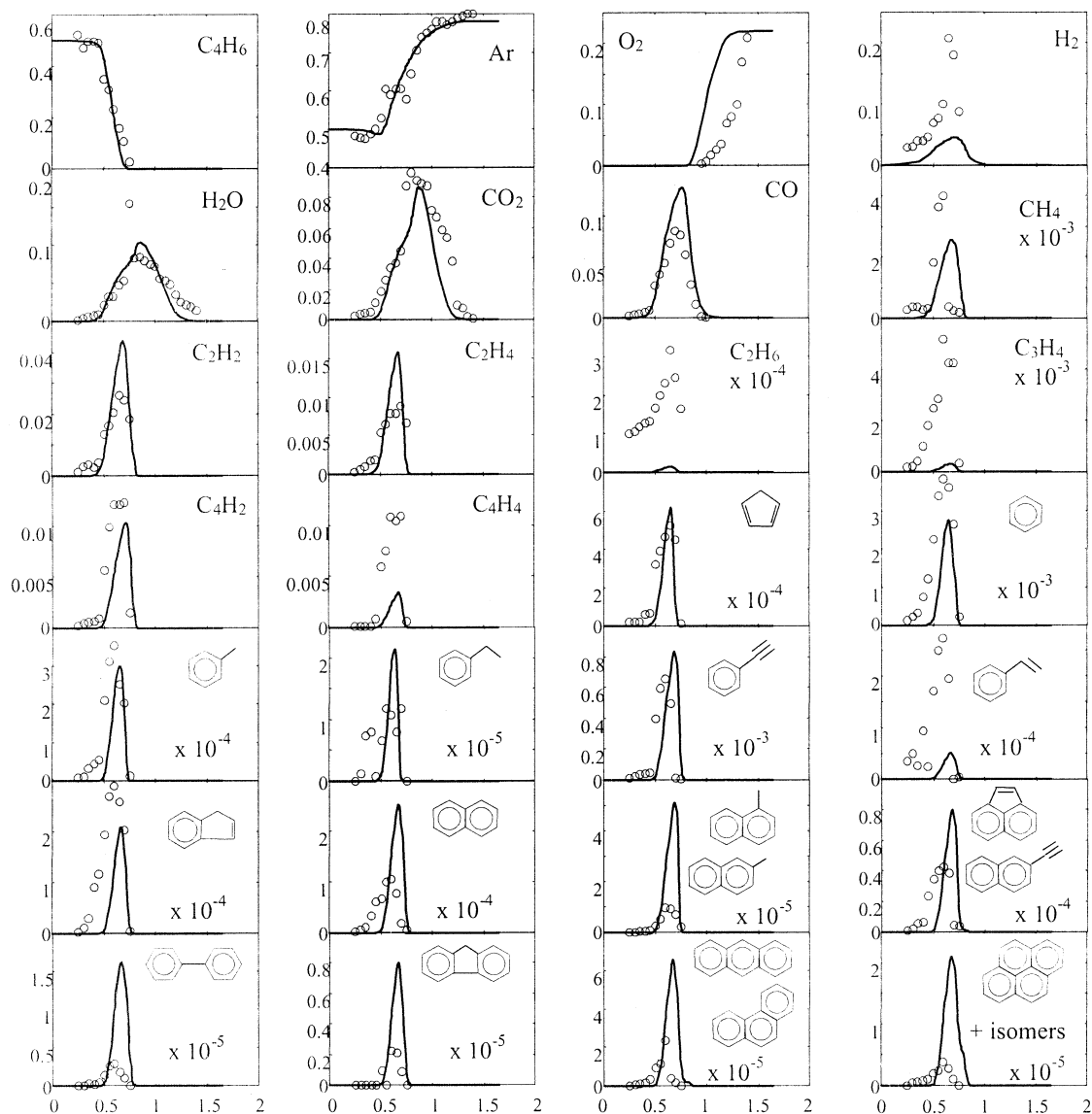
Fig. 2. Counterflow pure diffusion flame. Comparison between experimental (dots) and predicted (lines) mole fractions.

ously noted in Fig. 1, the maximum value in the predicted temperature profile largely exceeds the experimental one. Model predictions exhibited a limited sensitivity to this temperature discrepancy, until the location of the maximum temperature fully corresponds to the point of stoichiometric butadiene-oxygen ratio. On the other hand, if the experimental temperature profile without this coherence were specified, model predictions lose their consistency and very large discrepancies of the species profiles are observed. As an example, if the flame position theoretically evaluated is not

coherent with the measured temperature profile, higher temperatures in the rich zone increase the reactivity with a consequent enormous and unjustified formation of dehydrogenated species and heavy aromatic compounds.

As seen in Fig. 2, despite the large differences in the temperature profiles, the agreement between predicted and experimental data are quite reasonable. The concentration profiles of major species, up to cyclopentadiene, benzene, toluene and ethynylbenzene are successfully predicted by the model. On the other hand,
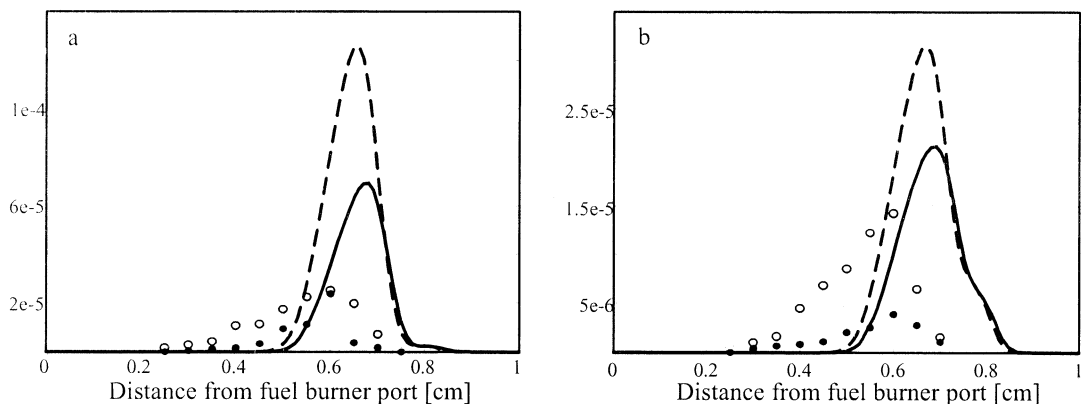
Fig. 3. Calculated and experimental mole fractions of phenanthrene (a) and pyrene and isomers (b) in the pure diffusion (solid lines and filled symbols) and in the doped (dashed lines and empty symbols) flame.

large discrepancies were observed between the experimental and predicted data of ethane, allene and propyne. Systematic over-predictions of the model are evident when considering naphthalene and heavier species such as phenanthrene and pyrene. These discrepancies can be explained, at least partially, on the basis of the simplifications of the adopted kinetic model, that is, the lack of detailed successive reactions to form heavier species. In fact, the proper description of heavy PAH species and soot formation requires the use of a larger number of heavier aromatic components and their relative reactions. Nevertheless, the indications coming from these comparisons are useful for a better understanding of the main paths up to PAH species. As already discussed in the previously referred paper [10], the experimental detail of heavy species up to four aromatic rings is very large. Because of the semi-detailed approach adopted in the kinetic model [11], the comparisons of Fig. 2 refer to lumped components. For instance, the predicted 'lumped pyrene' groups all the $C_{16}H_{10}$ components while the 'experimental' points are the sum of the experimentally detected isomers $C_{16}H_{10}$, where the true pyrene constitutes about the 60% and fluoroanthene is more than 30%. It has also to be underlined that such an experimental detail of PAH composition is quite difficult to be found in the literature, especially from counterflow flames.

Olten and Senkan report experimental details and species profiles [10] and find that when the fuel side is doped with O_2, PAH growth progressed further, forming cylopenta(cd)pyrene and its isomer benzo(ghi)fluoranthene as the largest detectable PAH. These PAH were not detected in the pure butadiene flame under similar conditions. Some oxygenated aromatic species, such as furan, benzaldehyde, and phenol, were also produced in the fuel side of the oxygen-doped flame, and with the exception of furan, all the other oxygenates reached their peak levels before the PAH.

It was not possible to numerically reproduce these experimental observations. All the calculated profiles, including temperature, slightly shifted toward the fuel side in the oxygen doped flame, but this effect was marginal in respect of the experimental one.

On the other hand, as shown in Fig. 3, the model specifically predicted an increase of three and four ring PAH in the oxygen doped flame. Experimental pyrene increase is in line with the calculations. Phenanthrene raise is less evident and is theoretically overestimated. The reaction paths analysis did not show a significant difference in the relative importance of the different paths between the pure diffusion and the oxygen doped flames. The reason of this behavior can be attributed to the larger number of radical species in the doped flame and consequently in an increase of the global reactivity.

The experimental data of benzene and naphthalene, showed lower peak concentrations and a wider distribution in the fuel zone for the O_2 doped flames. The numerical model was not
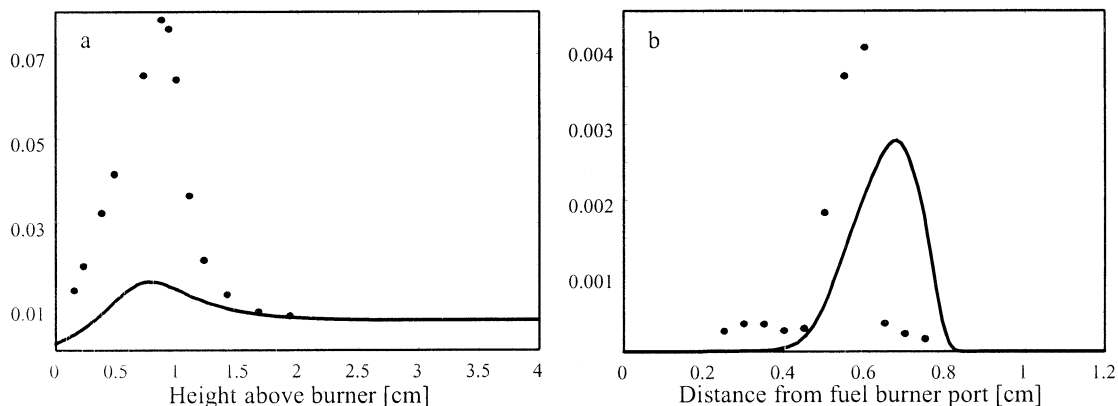
Fig. 4. Experimental and predicted mole fractions of methane. (a) Laminar premixed flame. (b) Counterflow diffusion flame.

successful in reproducing this effect. Even though these comparisons are still quite unsatisfactory, in our opinion it is important to analyze the discrepancies to highlight the model uncertainties and to indicate the need of further investigations.

The effect of oxygen addition in counterflow and co-flow flames has been investigated with ethylene fuel [29, 30]. With oxygen additions (up to 6%), aromatic species concentrations were found to increase with decreasing equivalence ratio. These findings are consistent with butadiene experimental results. For higher amount of oxygen the total PAH decreases, because of the oxidation effect. The fact that our model was not able to explain the reactivity observed in an O_2 doped flame at low temperatures, as experimentally evidenced by the formation of oxygenated aromatic species, calls for further kinetic mechanism work. Neither low temperature oxidation mechanism of butadiene nor a mechanism involving the HO_2 addition to butadiene (to form di-hydro-furan and benzaldehyde) were able to account for the observed reactivity and reaction products. In addition, we also examined concerted path molecular reactions between butadiene and oxygen without significant effect. Calculated temperatures and residence times in the zone of interest seem too low for these reaction mechanisms. It is entirely possible that some of the experimental data acquired in the O_2-doped flame can be experimental artifacts caused by heated surfaces of the sampling probe and transfer lines [31]. As a consequence of these issues from one side fur-

ther kinetic modeling work is needed to explain the unusual behavior of oxygen doped flame, from the other side new experiments in the intermediate temperature region should explain these observed discrepancies between model predictions and experimental results.

KINETIC ANALYSIS IN COUNTERFLOW DIFFUSION FLAMES AND LAMINAR PREMIXED FLAMES

As already mentioned, the aim of this paper is also to compare this counterflow diffusion butadiene flame with the results of the laminar premixed flame. As recently discussed [11], all the measured aromatic species are well predicted by the model in premixed flames [9]. On the contrary the model under predicts CH_4 by a factor of 4, as shown in Fig. 4. This large discrepancy was not observed in the counterflow diffusion flames, as shown in the same figure.

To better understand the situation, a reaction path analysis was performed to identify reactions that most significantly contribute to CH_4 formation. In Fig. 5, the reaction rate profiles of the most significant reactions involving CH_4 are presented. In premixed flames the following reaction:

$$HCO + CH_3 = CH_4 + CO$$
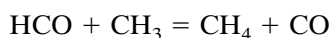
dominates methane formation [11]. CH_4 subsequently forms methyl by OH, O, and H radical H abstractions:
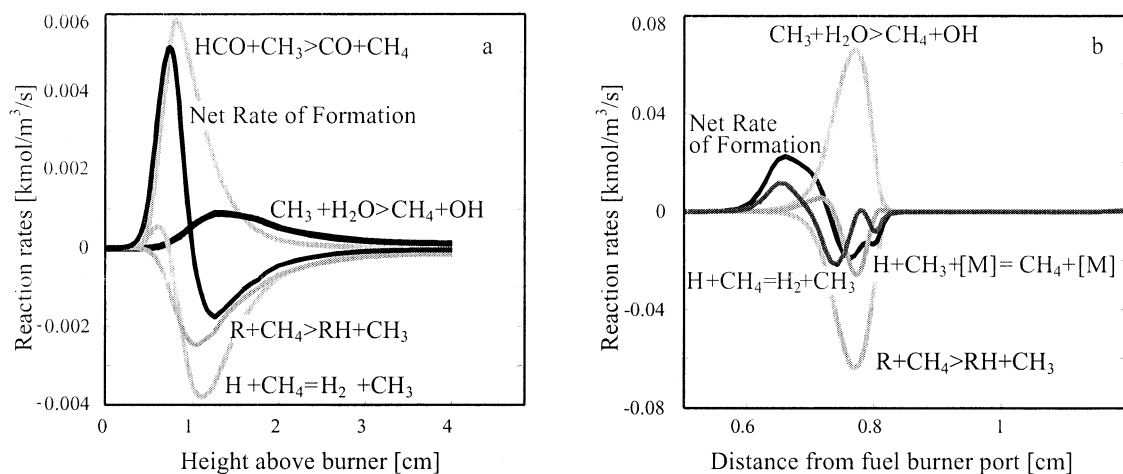
Fig. 5. Methane formation in the premixed flame (a) and in the pure diffusion flame (b).
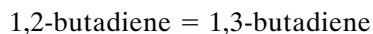
$$CH_4 + (OH, O, H) = CH_3 + (H_2O, OH, H_2)$$
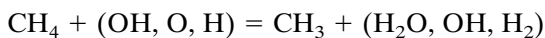
Evidently, the kinetics of the reactions used in the mechanism is not adequate to quantitatively predict the levels of CH_4 in the lower-pressure premixed flame of 1,3-butadiene. In contrast, methane formation in diffusion flames is governed by the hydrogenation of CH_3 radicals such as:
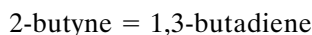
$$CH_3 + (H_2, RH) = CH_4 + (H, R)$$
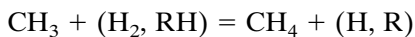
in the fuel rich sections of the flame, while the reverse processes govern CH_4 destruction in the later parts of the flame. The reaction flow analysis of methyl radical formation does not show primary sources directly involving butadiene as reactant and does not help the understanding of this deviation. The underprediction of methane, together with the slight C_2H_2 and C_2H_4 overprediction, indicates a possible erroneous branching ratio for the paths leading to C_2, C_3, and C_4 chemistry. The kinetic model, even though very large, remains a semi-detailed kinetic mechanism and several simplifications are assumed. First, only 1,3-butadiene is considered and the presence of both 1,2-butadiene and 1- and 2- butynes is disregarded. H addition reactions on 1,2-butadiene and on butynes could indeed explain the direct formation of methyl and C_3 species. To analyze the role of these reaction paths, we enlarged the kinetic scheme to include also 1,2-butadiene and 2-butyne with their major reactions. The chemistry

of 1-butyne was not included in the scheme because its equilibrium concentration never exceeds 0.5% of 1,3-butadiene at 1000 K, as clearly indicated by Laskin et al. [32]

Kinetic parameters suggested by Hidaka et al. [33] are adopted for the isomerization reactions:

1,2-butadiene = 1,3-butadiene

$k = 2.5 \times 10^{13} \exp(-63000/RT)$ $[s^{-1}]$

2-butyne = 1,3-butadiene

$k = 3 \times 10^{13} \exp(-65000/RT)$ $[s^{-1}]$

2-butyne = 1,2-butadiene
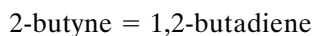
$k = 3 \times 10^{13} \exp(-67000/RT)$ $[s^{-1}]$

Moreover, the rate parameters of H addition reactions to form methyl and C_3 were taken from Hidaka et al. [33] and Lindstedt and Skevis [34]. Additional unimolecular decomposition of 1,2-butadiene and 2-butyne to form methyl and C_3H_3 were also included. Because of the very low concentration level of both these new C_4H_6 species, the effect of these reactions on methane and C_3H_4 formation was really very scarce and not sufficient to explain CH_4 deviations in the premixed flame.

H addition reactions on 1,3-butadiene to directly form methyl and C_3H_4s are not elementary steps. The kinetic model accounts for only two C_4H_7 radicals, the resonantly stabilized
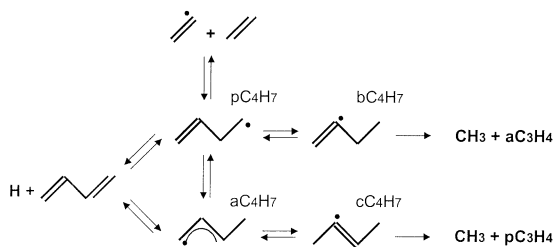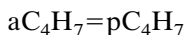
Fig. 6. H addition on 1,3-butadiene and successive reactions of C_4H_7 radicals.

(aC_4H_7) and the primary one (pC_4H_7). These radicals play a significant role in the steam cracking process reducing ethylene selectivity and contributing to the formation of aromatic species [22].

The butenyl radicals can isomerize:

$$aC_4H_7 = pC_4H_7$$
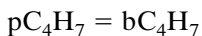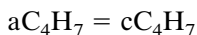
$$k = 6.5 \times 10^{12} \exp(-51800/RT) \quad [s^{-1}]$$

and decompose:

$$pC_4H_7 = C_2H_4 + C_2H_3$$

$$k = 2.5 \times 10^{13} \exp(-38000/RT) \quad [s^{-1}]$$

These kinetic parameters were discussed in a previous publication [22].

The possible isomers (bC_4H_7 and cC_4H_7), shown in Fig. 6, are not included in the scheme. These radicals are formed via isomerization reactions of aC_4H_7 and pC_4H_7:

$$pC_4H_7 = bC_4H_7$$

$$k = 3 \times 10^{11} \exp(-43000/RT) \quad [s^{-1}]$$

$$aC_4H_7 = cC_4H_7$$

$$k = 6 \times 10^{11} \exp(-52000/RT) \quad [s^{-1}]$$

The high activation energies estimated for both these reactions on the basis of simple additivity rules are because of the 1 to 3 and 1 to 2 H transfer (i.e., to the formation of a four and a three membered ring intermediate) and to the formation of vinyl type radicals [26]. Methyl formation, with allene and propyne respectively, could then be explained via β-decomposition reaction of bC_4H_7 and cC_4H_7. Unfortunately, also including these new radicals and reactions in the kinetic scheme, it is not possible to recover the observed deviations, at least with the adopted kinetics.

Reaction Paths Toward Benzene Formation

As shown in Fig. 7, the model predictions were in reasonable agreement with the experimental data for benzene both in premixed and in diffusion flames. In Fig. 8, the major elementary reactions contributing to benzene formation are presented.

In the premixed flame the addition reactions of vinyl radical on butadiene assume a large importance, as already verified in the typical steam cracking conditions [35] and also discussed in a recent paper [11]. More than 50% of benzene formation is because of this reaction. Even more favored is the second reaction channel with the formation of cyclopentadiene and methyl:
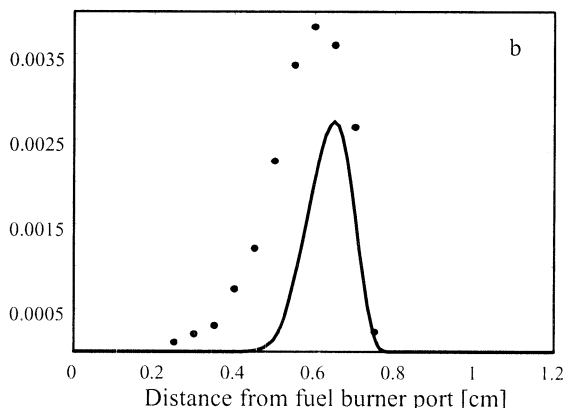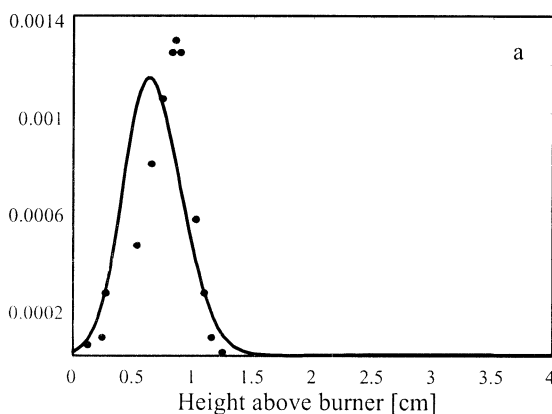

Fig. 7. Experimental and predicted mole fractions of benzene. (a) Laminar premixed flame. (b) Counterflow diffusion flame.
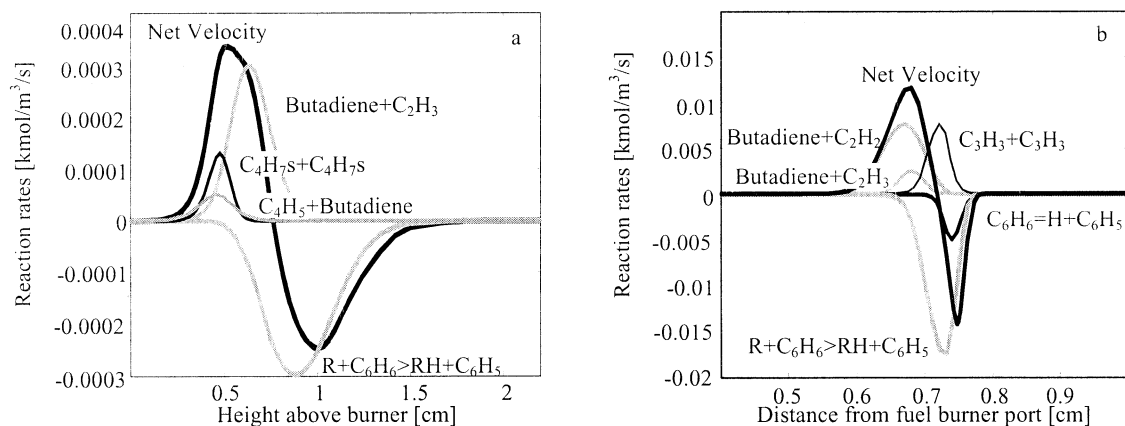
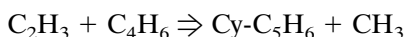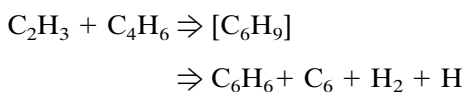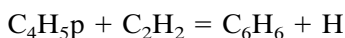Fig. 8. Benzene formation in the premixed flame (a) and in the pure diffusion flame (b).

$$C_2H_3 + C_4H_6 \Rightarrow [C_6H_9]$$
$$\Rightarrow C_6H_6 + C_6 + H_2 + H$$
$$C_2H_3 + C_4H_6 \Rightarrow Cy\text{-}C_5H_6 + CH_3$$

The latter reaction becomes important after the first 5 mm from the burner, when the vinyl radical concentration is large enough to sustain this reaction. Only in the very early stages direct $C_4 + C_4$ interactions and also C_4H_5 addition to acetylene play a role in benzene formation:

$$C_4H_7a + C_4H_7 \Rightarrow C_6H_6 + CH_3 + CH_3 + H_2$$
$$C_4H_5p + C_4H_6 \Rightarrow C_6H_6 + C_2H_3 + H_2$$
$$C_4H_5p + C_2H_2 = C_6H_6 + H$$
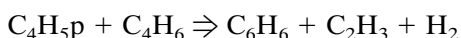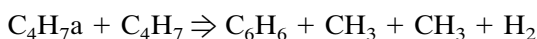
H abstraction from benzene by radical attack, mainly OH, were the most significant consumption reactions for benzene.

A similar match with experiments and a similar role of the C_2+C_4 reaction paths is also reported by Lindstedt and Skevis [34], even though they propose a large importance of linear C_6H_6.

Figure 8 also shows the major reaction paths of benzene formation in the pure diffusion flame. The first formation term in the fuel rich zone is the molecular addition of acetylene on butadiene with the formation of cyclohexadiene and the successive, very fast dehydrogenation reaction:

$$C_4H_6 + C_2H_2 \Rightarrow CyC_6H_8 \Rightarrow C_6H_6 + H_2$$

In this condition, the mechanism C_4+C_2 is the dominant one in the fuel rich zone. As a matter

of fact, the addition of vinyl radicals on butadiene also contributes for about 15%.

As already shown previously [36], the recombination reaction of propargyl radicals:

$$2\,C_3H_3 = C_6H_6$$
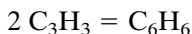
contributes to benzene formation only at high temperatures. Thus, this reaction pathway is unimportant in the fuel rich zone of the diffusion flames because of the low temperatures.

The major reasons of benzene consumption are the H abstraction reactions, mainly by H and OH radicals.

As already observed the presence of the small amount of oxygen does not modify significantly the reactive system, at least from the modeling point of view. As a consequence, reaction paths toward benzene are similar both in the pure diffusion and oxygen doped flames.

From this analysis it appears quite evident the presence of different kinetic paths in benzene formation in the diffusion and premixed flames because of the fuel-air mixing effect. This effect also manifests itself with the establishment of large differences in temperatures.

Reaction Paths Toward PAH Formation

Unfortunately, a complete experimental detail of PAH components is not available for the premixed flame and this precludes the possibility of a direct comparison.

In the case of counterflow flames, successive acetylene additions are as important as recom-
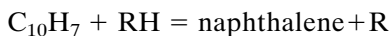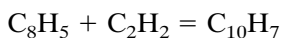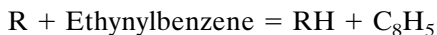
bination and condensation reactions of resonantly stabilized radicals, such as propargyl, cyclopentadienyl, benzyl, and indenyl.

Ethynylbenzene is a key component in the successive growth of PAH. HACA mechanism, via phenyl radical addition to acetylene is the main route to form ethynylbenzene and this reaction path explains more than 75% of benzene depletion. Ethynylbenzene is also formed (about 20–25%) by the addition of C_4H_5 radical to C_4H_2.

Model predictions of ethynylbenzene are very accurate, while styrene formation is under-estimated (Fig. 2).

Benzyl and indenyl radicals, together with propargyl and cyclopentadienyl radicals, also play an important role in subsequent PAH growth reactions. Indene is mainly formed via benzyl radical addition to acetylene.

About 50% of naphthalene comes from the recombination of cyclopentadienyl radicals, and propargyl with benzyl radicals. The remaining 40 to 50% is explained by the HACA mechanism:

$$R + Ethynylbenzene = RH + C_8H_5$$

$$C_8H_5 + C_2H_2 = C_{10}H_7$$

$$C_{10}H_7 + RH = naphthalene + R$$

HACA mechanism is also responsible of more than 50% of the sequential formation of acenaphthylene, phenanthrene, pyrene, and heavier species. The remaining fraction is explained by successive addition and recombination reactions of resonantly stabilized radicals.

As seen in Fig. 2, model predictions were generally in good agreement with the experimental data, even if a systematic over-prediction was present for species heavier than naphthalene. As already mentioned, a more detailed characterization of the heavy lumped aromatic species could further improve these predictions.

CONCLUSIONS

A semi-detailed kinetic scheme for the oxidation and pyrolysis of hydrocarbons was used to model the experimental data obtained in pure diffusion and premixed butadiene-oxygen flames. This effort involves a significant test of the mechanism because of the large variation in the local conditions present in these systems, both in terms of temperatures and C/O ratios. Moreover, the investigation of these counterflow diffusion flames is a further step toward the complete analysis and simulation of flame structures. The results show that the model agrees quite well with the experimental data especially for light species and one ring aromatic compounds. On the contrary, there is an over prediction of heavier PAH.

The reaction rate analysis also showed the large differences in the pathways characterizing the pollutant formation in the premixed flames when compared with the diffusive ones. This result confirms that there is a need to test the kinetic mechanisms developed and tuned for premixed conditions when they are extrapolated and used in diffusion flames. Therefore, although considerable future work remains, we believe that this joint activity from both the experimental and modeling perspectives is a fruitful cooperation to obtain a better understanding of the chemistry of combustion processes.

Thus, from one side experiments show the main areas where kinetic modeling studies require further efforts, from the other model predictions and deviations allow to address new attention to experiments in proper operating conditions.
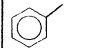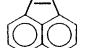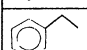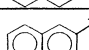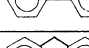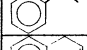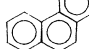
REFERENCES

1. Schalla, R. L., and McDonald, G. E., *Ind. Eng. Chem* 45:1947 (1953).
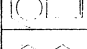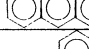2. Vaughan, W. E., *J. Am. Chem. Soc* 54:3863 (1932).
3. Kistiakovsky, G. B., and Ransom, W. W., *J. Chem. Phys* 7:725 (1939).
4. Harkness, J. B., Kistiakowski, G. B., and Mears, W. H., *J. Chem. Phys* 5:682 (1937).
5. Thomas, A., *Combust. Flame* 6:46 (1962).
6. Glasmann, I., and Yaccarino, P. *Eighteenth Symposium (International) on Combustion*, The Combustion Institute, Pittsburgh, 1981, p. 1175.
7. Smith, O. I., *Prog. Energy Combust. Sci* 7:275 (1981).
8. Tsang, W., *J. Chem. Phys* 42:1805 (1965).

9. Cole, J. A., Bittner, J. D., Longwell, J. P., and Howard, J. B., *Combust. Flame* 56:51 (1984).

10. Olten, N., and Senkan, S., *Combust. Flame* 125:1032 (2001).

11. Goldaniga, A., Faravelli, T., and Ranzi, E., *Combust. Flame* 122:350 (2000).

12. Miller, J. A., and Melius, C. F., *Combust. Flame* 91:21 (1992).

13. Marinov, N. M., Pitz, W. J., Westbrook, C. K., Castaldi, M. J., and Senkan, S. M., *Combust. Sci. Tech* 116–117:211 (1996).

14. Olten, N., and Senkan, S., *Combust. Flame* 118:500 (1999).

15. Olten, N., and Senkan, S., *Combust. Sci. Tech* 159:1 (2000).

16. Lutz, A. E., Kee, R. J., Grcar, J. F., and Rupley, F. M., *OPPDIF: A Fortran Program for Computing Opposed Flow Diffusion Flames*. Sandia Report, SAND96-8243, (1997).

17. Kee, R. J., Grcar, J. F., Smooke, M. D, and Miller, J. A., *PREMIX: A Fortran Program for Modeling steady Laminar One-dimensional Premixed Flames*. Sandia Report, SAND85-8240, (1985).

18. Ranzi, E., Dente, M., Goldaniga, A., Bozzano, G., and Faravelli, T., *Prog. Energy Combust. Sci* 27:99 (2001).

19. Marinov, N. M., Pitz, W. J., Westbrook, C. K., Lutz, A. E., Vincitore, A. M., and Senkan, S. M., *Twenty-seventh Symposium (International) on Combustion*, The Combustion Institute, Pittsburgh, 1998, p. 605.

20. Goldaniga, A., Granata, S., Rivolta, E., et al., *Open Meeting on Combustion*. Ischia, 2000.

21. Ranzi, E., Faravelli, T., Gaffuri, P., Sogaro, A., D'Anna, A., and Ciajolo, A., *Combust. Flame* 108:24 (1997).

22. Dente, M., Ranzi, E., and Goossens, A. G., *Comp. Chem. Engng* 3:61 (1979).

23. Appel, J., Bockhorn, H., and Frenklach, M., *Combust. Flame* 121:122 (2000).

24. Kee, R. J., Rupley, F. M., and Miller, J. A., *The Chemkin thermodynamic data base*. Sandia Report, SAND87–8215B, (1987).

25. Burcat, A., and McBride, B., *Ideal Gas Thermodynamic Data for Combustion and Air-Pollution Use*. Technion Israel Institute of Technology, Aerospace Engineering Report, TAE804, (1997).

26. Benson, S. W., *Thermochemical Kinetics,* 2nd edn. John Wiley and Sons, New York, 1976.

27. Kee, R. J., Dixon-Lewis, G., Warnatz, J., Coltrin, M. E, and Miller, J. A., *The Chemkin Transport Data Base*. Sandia Report, SAND86-8246, 1986.

28. Wang, H., and Frenklach, M., *Combust. Flame* 96:163 (1994).

29. Hwang, J. Y., Chung, S. H., and Lee, W., *Twenty-seventh Symposium (International) on Combustion*. The Combustion Institute, Pittsburgh, 1998, p. 1531.

30. McEnally, C. S., and Pfefferle, L. D., *Combust. Flame* 121:575 (2000).

31. Huang, J. W., and Senkan, S., *Twenty-sixth Symposium (International) on Combustion*. The Combustion Institute, Pittsburgh, 1996, p. 2335.

32. Laskin, A., Wang, H., and Law, C. K., *Int. J. Chem. Kinet* 32:589 (2000).

33. Hidaka, Y., Higashihara, T., Ninomiya, N., Oshita, H., and Kawano, H., *J. Phys. Chem* 97:10977 (1993).

34. Lindstedt, P, and Skevis, G., *Twenty-sixth Symposium (International) on Combustion*. The Combustion Institute, Pittsburgh, 1996, p. 703.

35. Dente, M., and Ranzi, E., *Pyrolysis: Theory and Industrial Practice* (L. F. Albright, B. L. Crines, and W. H. Corcoran Eds.), Academic Press, San Diego, 1983.

36. Faravelli, T., Goldaniga, A., and Ranzi, E., *Twenty-seventh Symposium (International) on Combustion*, The Combustion Institute, Pittsburgh, 1998, p. 1489.

APPENDIX

	Benzene		2-Methylnaphthalene
	Toluene		Acenaphthylene
	Ethylbenzene		Ethynylnaphthalene
	Ethynylbenzene		Biphenyl
	Styrene		Fluorene
	Indene		Anthracene
	Naphthalene		Phenanthrene
	1-Methylnaphthalene		Pyrene